Elastic Born modeling in an ocean-bottom node acquisition scenario

Ohad Barak

ABSTRACT

PZ summation is a common method for separating the upgoing wavefield from the downgoing wavefield in data acquired by four-component ocean-bottom node surveys. It assumes that the vertical geophone component records mostly pressure waves. If this assumption is not satisfied, non-pressure wave energy (such as shear waves) will be introduced as pressure waves into the receiver wavefield, which may generate artifacts in the migration image. I formulate an elastic Born modeling and migration method for ocean-bottom node acquired data. I then use a synthetic example to demonstrate the effect of the introduction of non-pressure wave energy into the receiver data on the resulting image.

INTRODUCTION

In four-component ocean-bottom node (OBN) acquisition, the pressure wave is recorded by a hydrophone suspended in the water layer just above the sea floor. Additionally, three-component geophones are attached to the sea floor and record the vertical and two perpendicular horizontal particle velocities. The source is an airgun fired at the water surface. The upgoing wave can be distinguished from the downgoing wave by comparing the vertical geophone data to the hydrophone data. Whereas in the hydrophone data both the downgoing and the upgoing wave will have a positive polarity (assuming positive reflection coefficients in the subsurface), the value of the geophone data depends on the wave's vertical propagation direction. The downgoing wave will register on the vertical geophone with a negative polarity, while the upgoing wave will have a positive polarity.

This characteristic has led to the PZ summation methodology (Barr and Sanders, 1989). With a proper scaling factor, the sum of the hydrophone and the vertical geophone should result in the upgoing waves only, while their difference should yield the downgoing wave only. This differentiation between the energy propagation direction at the sea floor has several applications. One of these applications is the ability to create separate images of the upgoing waves and of the downgoing waves that are reflected off the water surface, also known as the "mirror-image" (Ronen et al., 2005; Wong et al., 2009).

The PZ summation methodology, however, assumes that the energy recorded in the hydrophone and in the vertical geophone is mostly pressure wave energy. For the

hydrophone, since it is within the water column, this assumption holds. However, if significant amounts of other wave modes are recorded by the geophone, then the PZ summation will not handle them properly, and will in effect introduce them into either the upgoing or the downgoing field. The sketch in Figure 1 displays this issue for the case where PZ summation is used to extract the upgoing data. Later processing steps (such as mirror-imaging), which rely on the assumption that the separated upgoing or downgoing data contains only acoustic arrivals, may have their results affected in turn.

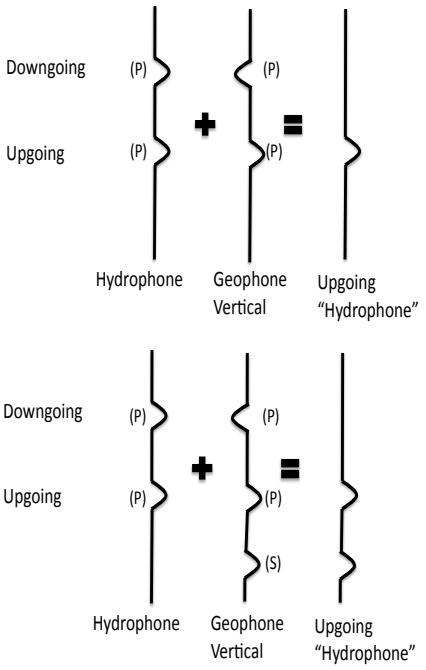

Figure 1: Simplified sketch of PZ summation. Top: For acoustic data, the summation of the hydrophone data and the vertical geophone data will result in the downgoing energy being eliminated, leaving only upgoing pressure data. Bottom: If the data contains shear waves, they will be recorded only by the geophone, and the PZ summation will mistakingly insert them into the result as upgoing pressure data. [**NR**]

In this paper I show the effect of imperfect PZ summation, as a result of significant shear wave energy existing in the vertical geophone, on the imaging of the upgoing wavefield.

In order to create single-scattered OBN synthetic data and run RTM with such data as input, I formulated and coded an elastic Born modeler. The special case of OBN acquisition necessitated a special manipulation of the smooth and the perturbed velocity models required to carry out Born modeling. The geophone receiver data was synthesized by recording the particle velocities of the single-scattered wavefield at the sea bed, and the hydrophone data was synthesized by recording the average of the normal stresses just above the sea bed, in the water-column.

The elastic propagation code is two dimensional, and all following examples are 2D as well. The gridding method I used for the elastic propagation was the Virieux staggered grid (Virieux, 1986), in which some wavefield values are located at grid points, and some are located at half-grid points, both spatially and temporally. The actual values which are propagated are the normal and transverse stresses $(\sigma_{xx}, \sigma_{zz}, \sigma_{xz})$, and the vertical and horizontal particle velocities (v_x, v_z). The P and S wavefields

are extracted from the particle velocity fields by applying either the divergence or the curl operator to them, respectively.

For imaging of the P and S-wave modes in the elastic source and receiver wavefields, I follow the vector potential imaging condition discussed in Yan and Sava (2008). As they mention, the imaging results for full elastic propagation suffer from spurious modes being created when particle velocity data are injected as a boundary condition into the receiver wavefield during elastic RTM. In other words, injection of recorded P-wave particle velocities in an elastic medium will invariably create a P-wave and an S-wave mode. These injected spurious modes will, at the imaging stage, give rise to artifacts. This problem is similar to the problem of multiple generation in the receiver wavefield when a non-smooth model is used.

There are more advanced methods for achieving both up/down separation in conjunction with P/S separation, in the data domain. Dankbaar (1985), Wapenaar et al. (1990), Amundsen (1993) and Schalkwijk et al. (2003) have all shown methods which can separate pressure and shear waves in the data, as well as separating upgoing from downgoing. However these methods require good knowledge of medium parameters at the sea bed where the geophones are located. Furthermore, it is not correct to assume that the data are composed of pressure and shear body waves only. In OBN acquisition (as in land acquisition) surface waves can contaminate the data.

PZ SUMMATION

PZ summation involves summing the pressure data recorded by the hydrophone data with the vertical particle velocity data recorded by the geophone, with some scaling factor:

$$\begin{aligned} U(z_r) &= \frac{1}{2}\left[P(z_r) - \beta V_z(z_r)\right], \\ D(z_r) &= \frac{1}{2}\left[P(z_r) + \beta V_z(z_r)\right], \end{aligned} \tag{1}$$

where P is the pressure data, V_z is the vertical particle velocity, U is the upgoing data, D is the downgoing data and z_r is the receiver depth. β is a scaling factor, which can be defined in several ways. Amundsen (1993) does the separation in the $f-k$ domain, and uses $\beta = \frac{\rho\omega}{k_z}$, where $k_z = \sqrt{\frac{\omega^2}{v^2} - k_x^2 - k_y^2}$, and ρ is the density. Alternately in the $t-x$ space, the scaling can be determined by the ratio of the direct arrival's amplitude on the hydrophone and vertical geophone components at various offsets.

As mentioned above, this method assumes that all energy is pressure wave energy, and therefore everything recorded by the hydrophone has its counterpart in the geophone data, with either positive polarity (upgoing) or negative polarity (downgoing). Shear waves, on the other hand, can only propagate upwards, since they are generated by mode conversions in the subsurface. They can have a very different polarity

upon reaching the sea bed, which can change differently with offset in comparison to the P-wave polarity. Running PZ summation on data that contains significant shear wave energy (or indeed - significant amounts of anything that is not pure P body waves) introduces events into the separated data fields, which will be construed by later processing steps as either upgoing or downgoing P-wave energy.

ELASTIC BORN MODELING

The elastic isotropic wave equation in index notation reads:

$$\partial_i \sigma_{ii} + \partial_j \sigma_{ij} + f_i(\mathbf{x}, t) = \rho \partial_t v_i, \tag{2}$$

where σ_{ii} are the normal stresses, σ_{ij} are the transverse stresses, f_i is the source function in direction i, $\mathbf{x}$ is the spatial source location operating at time t, ρ is density and v_i is the particle velocity in direction i. The stresses are propagated using the stress-displacement relation:

$$\begin{aligned} \sigma_{ii} &= (\lambda + 2\mu)\partial_i v_i + \lambda \partial_j v_j, \\ \sigma_{ij} &= \mu \left(\partial_j v_i + \partial_i v_j \right), \end{aligned} \tag{3}$$

where λ and μ are the Lame elastic constants.

In the staggered time grid methodology for elastic propagation (Virieux, 1986) the stresses and particle velocities are always half a time step apart. Therefore equation 2 and equation 3 are solved in alternation during the propagation.

For elastic Born modeling, these equations must be linearized. Beylkin and Burridge (1990) show a full derivation of linearized scattering for an elastic solid. Using $r = \frac{1}{\rho}$ to denote the specific volume, we have three models for the elastic isotropic case:

$$r = r^0 + \Delta r, \quad \lambda = \lambda^0 + \Delta\lambda, \quad \mu = \mu^0 + \Delta\mu, \tag{4}$$

where λ^0, μ^0 and r^0 are the smooth models, and $\Delta\lambda$, $\Delta\mu$ and Δr are the perturbed models.

We also have the incident and scattered stress and particle velocity fields:

$$v_i^0, \quad \Delta v_i, \quad \sigma_{ij}^0, \quad \Delta\sigma_{ij} \tag{5}$$

The incident stress and particle velocity fields need to propagated with the smooth models so that they do not generate reflections. At each time step, the perturbed models must be multiplied by these incident fields, and then injected as an additive source function into the scattered fields. As a result of the staggered time grid, the injection must be done alternately into the stress and particle velocity fields. The scattered fields themselves must also be propagated with the smooth models, so that they do not generate any additional scattering.

Low shear velocities at the water-solid boundary

The special case of OBN acquisition presents a unique problem for elastic Born modeling. Shear velocity in the water column is zero. In the shallow sediment, while not being very high, the shear velocity is necessarily not zero. The smoothing of the shear velocity model near the water-solid interface means that very small shear velocity values exist in the model. These in turn give rise to extremely short wavelengths, which require very fine gridding in order to spatially sample them properly and avoid dispersion effects. This issue is doubly important for OBN, since the water-solid interface is where the receivers are located, meaning that any dispersion in the modeling will have a direct effect on the synthesized data, and on the reverse propagated wavefields. I've found one possible temporary solution to this problem: use two separate smooth models, one for the incident wavefield and one for the scattered wavefield. Using Θ to denote the group of medium paramers, we have:

Incident smooth models: $\Theta_I^0 = [r_I^0, \quad \lambda_I^0, \quad \mu_I^0]$.
Scattered smooth models: $\Theta_S^0 = [r_S^0, \quad \lambda_S^0, \quad \mu_S^0]$.
Perturbed models: $\Delta\Theta_S = [\Delta r_S, \quad \Delta\lambda_S, \quad \Delta\mu_S]$.

Figures 2(a)-2(c) show these three model versions for the μ parameter.

For the incident wavefield, the model is smoothed everywhere except for the water-solid interface (Figure 2(a)). For the scattered wavefield, the topmost sediment's model replaces the water column (Figure 2(b)). The perturbed models are the difference between the "true" scattered model (water replaced by solid) and the smooth scattered model. Therefore, the perturbed models do not include the water-solid boundary (Figure 2(c)), and as a result no reflection is generated in the scattered wavefield at the sea bed. There is, however, a reflection generated in the incident wavefield at the water bottom, which admittedly is exactly the way Born modeling is not supposed to work. The water-solid substitution also causes wrong kinematics of the scattered wavefield in the water column. Neither of these issues affect the results since all energy is absorbed at the model boundaries, eliminating any free-surface multiples. A different solution will have to be found at a later stage if I wish to incorporate free-surface multiples into the processing.

WAVE MODE SEPARATION AND IMAGING

The Helmholtz amplitude separation is based on the assumption that any isotropic vector field can be described as a combination of a scalar and vector potential fields:

$$\mathbf{u} = \nabla\Phi + \nabla \times \mathbf{\Psi}, \tag{6}$$

Where Φ is the scalar potential field and $\mathbf{\Psi}$ is the vector potential. $\mathbf{u}$ is the elastic displacement vector wavefield. The scalar potential generates pressure waves, and the vector potential generates shear waves. Therefore, the Helmholtz method of

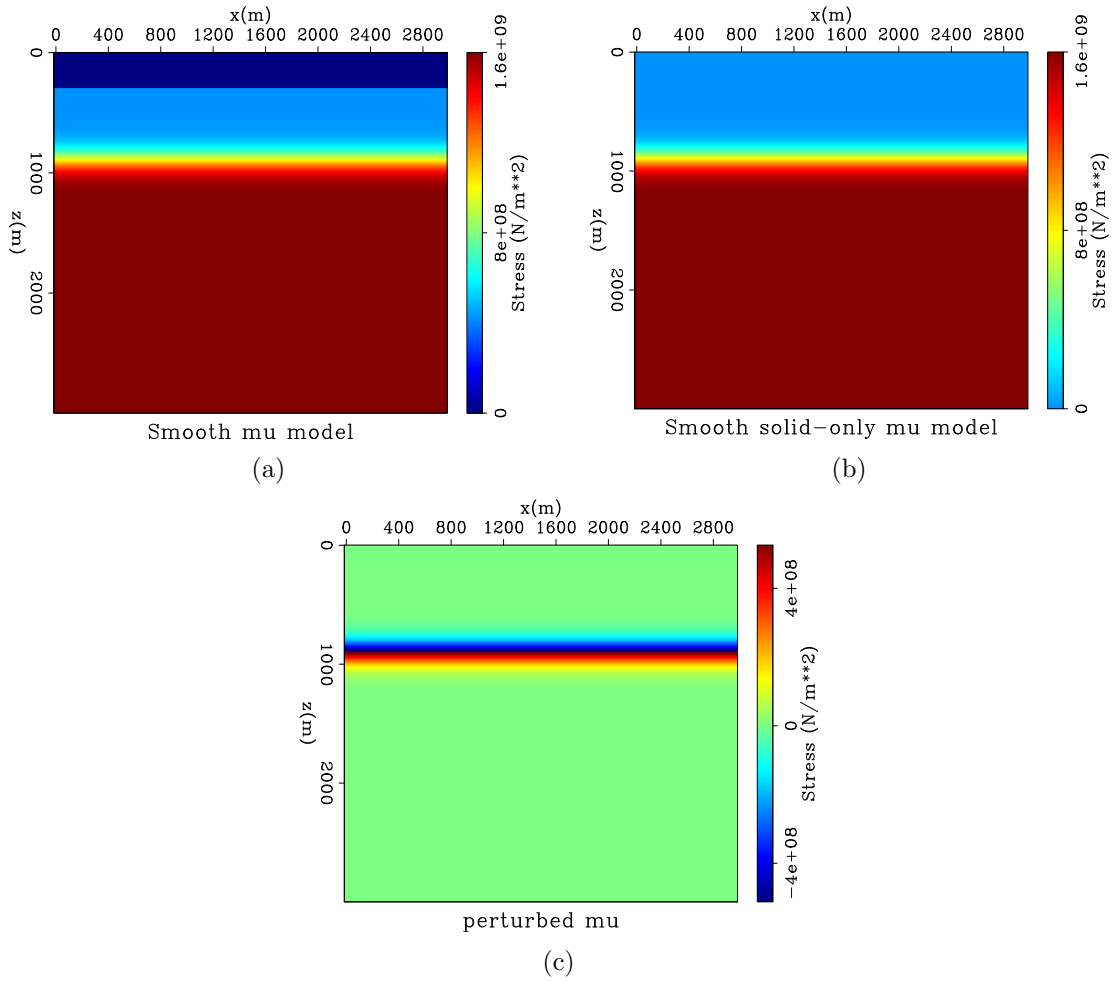

Figure 2: Top left: Smooth model for incident wavefield. Note the sharp water-solid boundary. Top right: Smooth model for scattered wavefield, where the water has been replaced by the topmost layer. Bottom: The perturbed model, which is the difference between the true model without the water layer and the smooth model without the water layer. Note the lack of a perturbation at the sea bed. [**ER**]

separating the P-wave amplitude from the S-wave amplitude is to apply a divergence operator and a curl operator to the displacement field:

$$P = \nabla \cdot \mathbf{u} = \nabla^2 \Phi; \tag{7}$$

$$\mathbf{S} = \nabla \times \mathbf{u} = -\nabla^2 \Psi. \tag{8}$$

Equations 7 and 8 work only for an isotropic medium. Dellinger and Etgen (1990) extend these operators for an anisotropic medium. Yan and Sava (2008) use these separated P and S-wave modes to formulate an imaging condition for vector potentials in an isotropic medium:

$$I_{ij}(\mathbf{x}) = \int_t \alpha_{si}\left(\mathbf{x}, t\right) \alpha_{ri}\left(\mathbf{x}, t\right) dt, \tag{9}$$

where the indices i, j denote the wave mode (P or S) of the wavefield α, and s, r denote the source and receiver fields. Therefore $I_{PP}(\mathbf{x})$ represents the cross-correlation of the source P field with the receiver P field, while $I_{PS}(\mathbf{x})$ represents the cross-correlation of the source P field with the receiver S field. In addition to the conventional PP image, the PS image can supply more information regarding medium parameters. This does, however, depend on the quality of the shear wave data, and on the accuracy of the acoustic velocity, shear velocity and density models.

MODELING AND MIGRATION RESULTS

Elastic Born forward modeling

In the following examples, I used a 3 layer 1D model of acoustic velocity, shear velocity and density. The top layer was water, and there was a full spread of receivers located at the water bottom. Figure 3 represents the models used for the incident wavefield (sharp water bottom interface). In the models used to propagate the scattered wavefield, the layer marked "sediment 1" is extended all the way to the surface. The model parameters were:

$\rho_1 = 1025 \frac{kg}{m^3}$ $V_{p1} = 1500 \frac{m}{s}$ $V_{s1} = 0 \frac{m}{s}$
$\rho_2 = 1700 \frac{kg}{m^3}$ $V_{p2} = 1700 \frac{m}{s}$ $V_{s2} = 500 \frac{m}{s}$
$\rho_3 = 1600 \frac{kg}{m^3}$ $V_{p3} = 2200 \frac{m}{s}$ $V_{s3} = 1000 \frac{m}{s}$

Figures 4(a)-4(l) show the incident and scattered P and S wavefields, which are a result of the application of equations 7 and 8 to the Born-modeled incident and scattered particle velocity fields. The rows are arranged by time snapshots, so at each row we see each field at the same time. The column order from left to right is incident P, scattered P, incident S, scattered S. In Figure 4(a) we can see the P reflection at the water bottom, resulting from the sharp boundary there. This

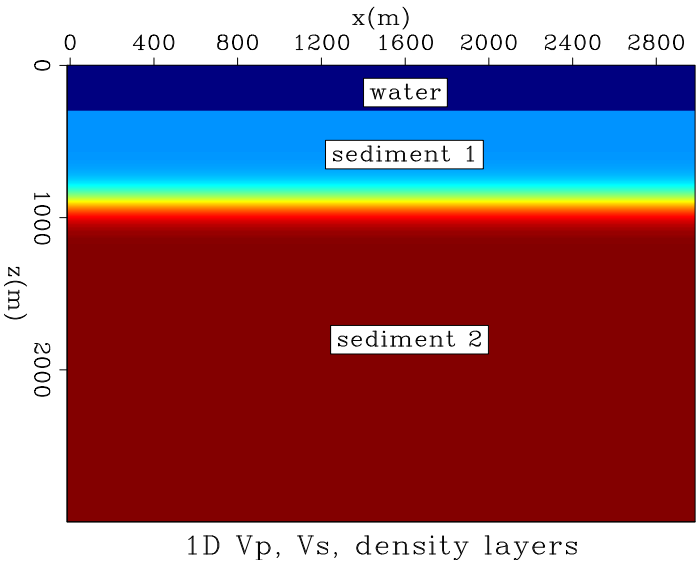

Figure 3: The smooth ρ, V_p and V_s model representation for the incident wavefield. [**ER**]

reflection is absorbed by the attenuating boundaries. In Figure 4(b) and 4(f), the P reflection from the bottom reflector is visible. Figure 4(c) is the incident S-wave generated by mode conversion at the water-solid interface. Figures 4(d) and 4(h) show the scattered S-wave generated by a mode conversion at the bottom reflector. Figures 4(e) and 4(i) are the propagating incident P wavefield. In Figure 4(g), though it is the incident S field, we can still see a transmitted mode conversion from the incident P wavefield at the bottom reflector. In Figure 4(k), the S-wave has hit the bottom reflector, which is the reason that we see both a P and an S reflection in the scattered field in Figures 4(j) and 4(l).

The simulation of OBN hydrophone recording is done by saving the scattered P wavefield one model cell above the sea bottom. The horizontal and vertical geophone recording is done by saving the vertical and horizontal particle velocity fields, within the solid layer at the sea bottom. The receivers are fully spread on the sea bottom. The source is an explosive source at the sea surface.

Figure 5 shows the recorded data components, generated by the elastic Born modeling. There is no direct arrival, since the water-solid interface is not used to generate scattering. Note that the shear wave recording is virtual. There is no recevier that records only shear waves. However, using equation 8 the shear wave value can be extracted from the particle-velocity fields at the sea bed. This information is useful for analyzing which of the reflections are P and which are S. The reflection types are pointed out in the figure. The label "PP" signifies a P-wave generated at the source position, which was transmitted at the water bottom as a P-wave, and was reflected as a P-wave at the bottom reflector within the sediment (Figure 3). The label "PS" signifies a similar path, except that at the bottom reflector a mode conversion occures, resulting in an upgoing S-wave. The label "SP" signifies a P-wave generated at the source position, which was converted at the sea bottom to a transmitted S-wave, and was converted again upon reflection at the bottom reflector to an upgoing P-wave.

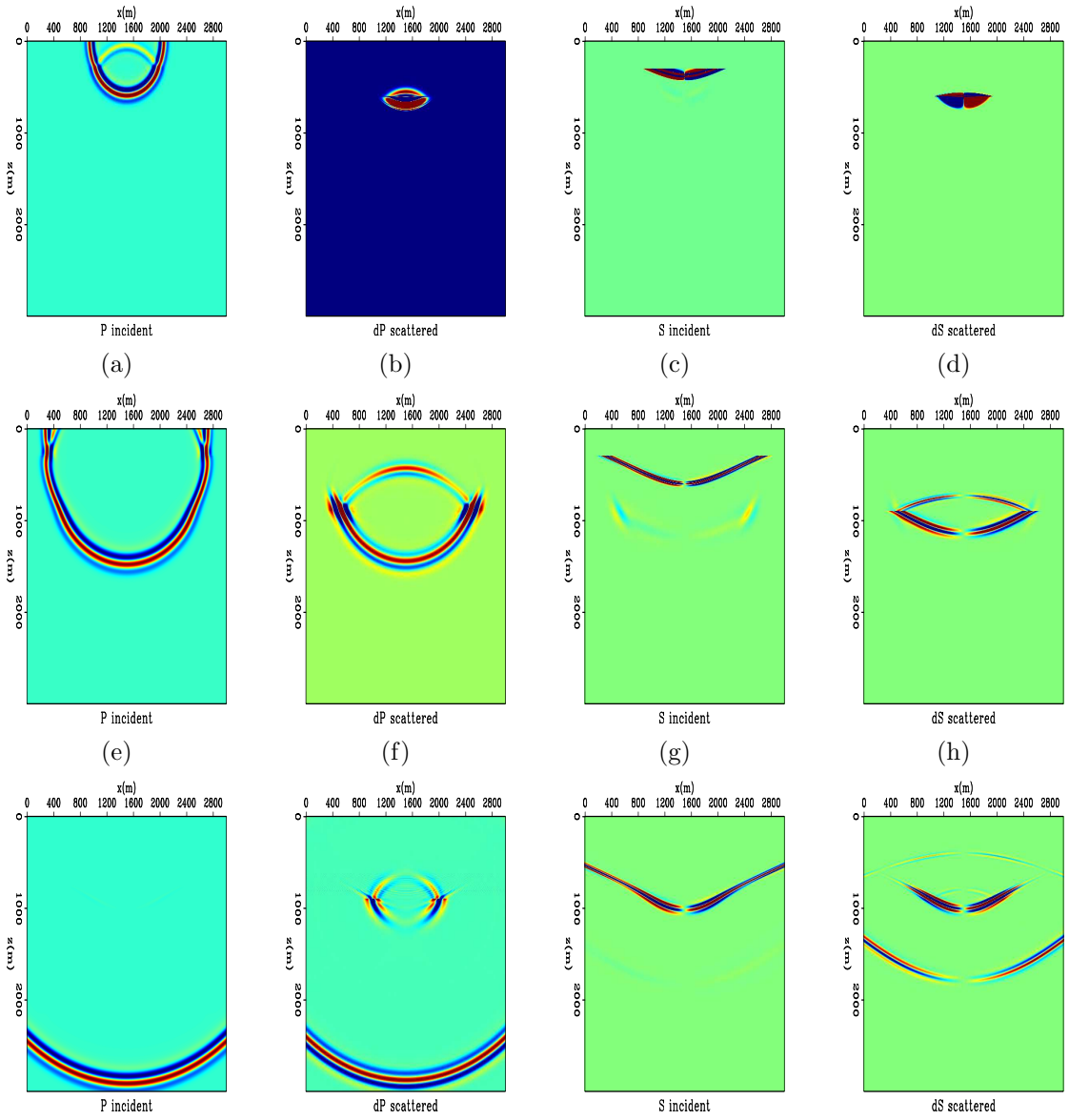

Figure 4: P and S incident and scattered wavefield snapshots at propagation times: t1=0.46s (top row), t2=0.9s (center row), t3=1.55s (bottom row). [**ER**]

Observing the hydrophone data and the virtual shear wave recording, we can see that the vertical and radial geophone components record both P and S-waves. Furthermore, we can see that the arrival at $t = 1.8s$ contains two converted modes: PS and SP. They arrive at the same time, since the model is 1D. As a result of the single-scattering of the Born modeler, all data in Figure 5 are upgoing data, and therefore represent the result we expect to have from a perfect separation of the upgoing from the downgoing wavefields.

Figure 6 is the recording of data generated by acoustic Born modeling. In effect, I used the same code as for the elastic modeling, setting $V_s = 0$. This is the reason for the empty data in the virtual shear wave recording. As expected, there is only one PP arrival. Again - no direct wave is visible since the water-solid interface is not used to generate scattering. Like the previous elastic data example, this upgoing acoustic recording is what we expect from a perfect up/down separation.

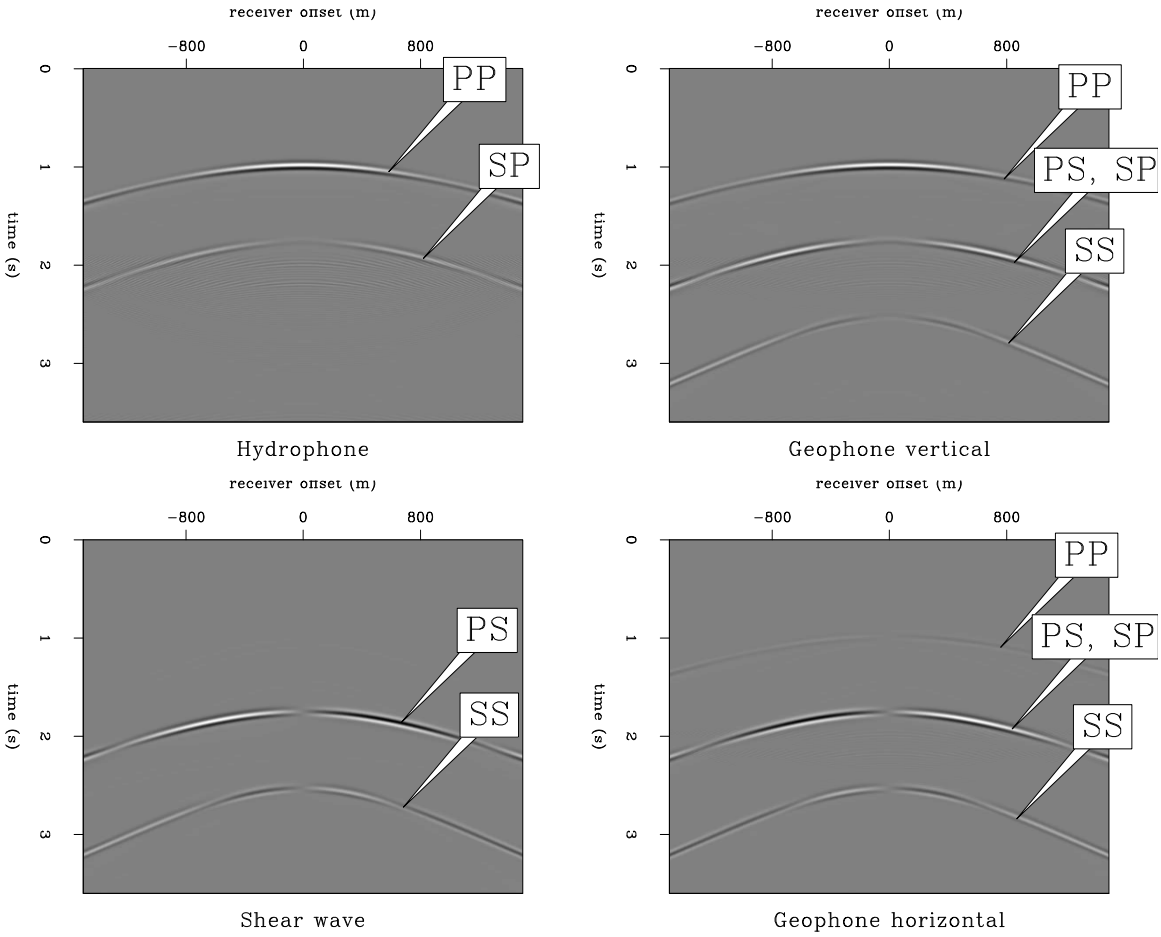

Figure 5: Synthetic OBN data generated by elastic Born modeling. Top left: Hydrophone containing only P-wave data. Top right: Vertical geophone containing P and S-wave data. Bottom left: Shear wave virtual recording. Bottom right: Horizontal geophone containing P and S-wave data. Note the lack of a direct arrival, as a result of the water-solid interface not being used to generate scattering. [**ER**]

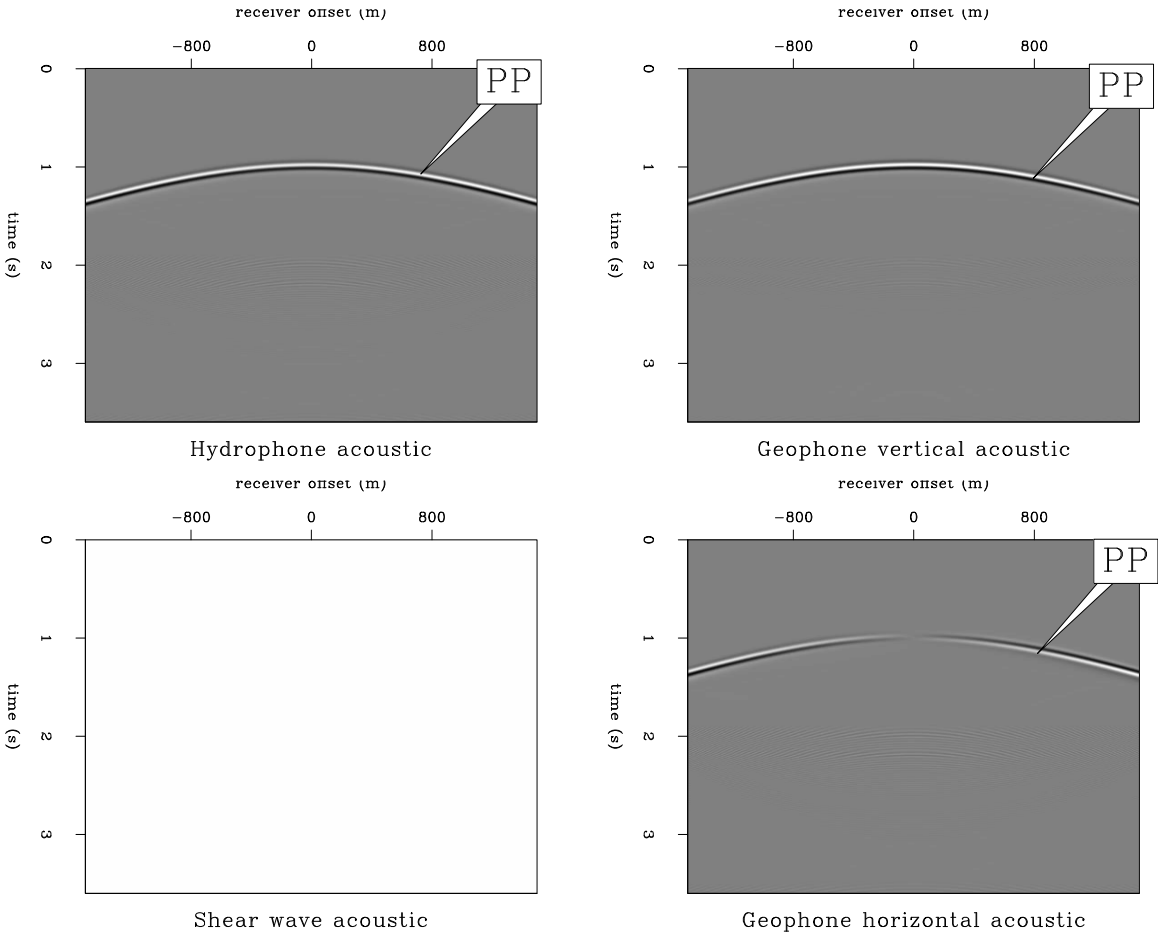

Figure 6: Synthetic OBN data generated by acoustic Born modeling. Top left: Hydrophone containing only P-wave data. Top right: Vertical geophone containing only P-wave data. Bottom left: Shear wave virtual recording. Bottom right: Horizontal geophone containing only P data. [**ER**]

PZ summation and imaging of pure and converted wave modes

PZ summation operates on the hydrophone and the vertical geophone component. Looking at figure 5, we can see that were we to use PZ summation, the PS and the SS arrivals would be introduced into the summation result. This effect is shown in the left panel of Figure 7. I scaled the geophone data to match the first reflection event of the hydrophone data (which is a PP reflection), and then took the average of the vertical geophone and hydrophone, which is equivalent to applying equation 1. In a standard processing flow, this result of PZ summation would be treated as acoustic data, and migrated with an acoustic velocity. The left panel of Figure 8 is the result of acoustic reverse time propagation of the PZ-summed hydrophone data, followed by a cross-correlation with an acoustically propagated source wavefield, and then a stacking over sources to improve the signal-to-noise ratio. The source and receiver wavefields are propagated with a smooth velocity model so that no receiver-side multiples are generated. Two artifacts are visible below the true reflector position. These artifacts come from the cross-correlation of the SS and the PS reflection events, which were brought into the acoustic data by PZ summation, with the acoustic source wavefield.

In a perfectly acoustic medium, the result of PZ summation would be just the PP reflection event, as can be seen on the right panel of Figure 7. Executing acoustic RTM with a smooth acoustic velocity model and the right panel of Figure 7 as input, we get the artifact-free image on the right panel of Figure 8.

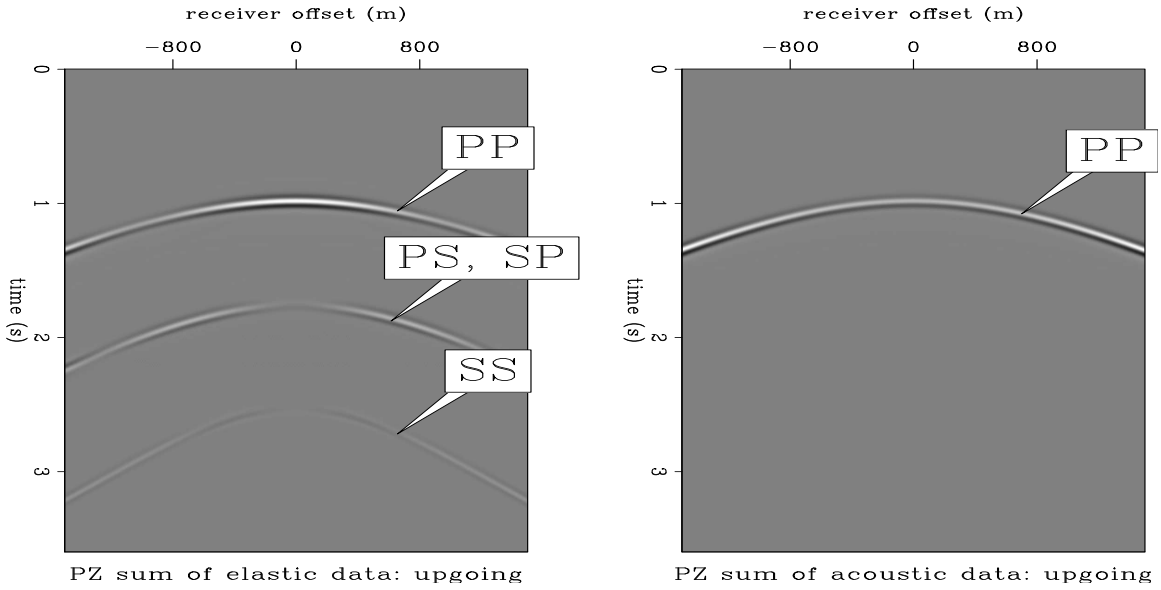

Figure 7: Result of PZ summation of elastically generated data (top) vs. acoustically generated data. The summation introduces the non-P energy into the upgoing data. [**ER**]

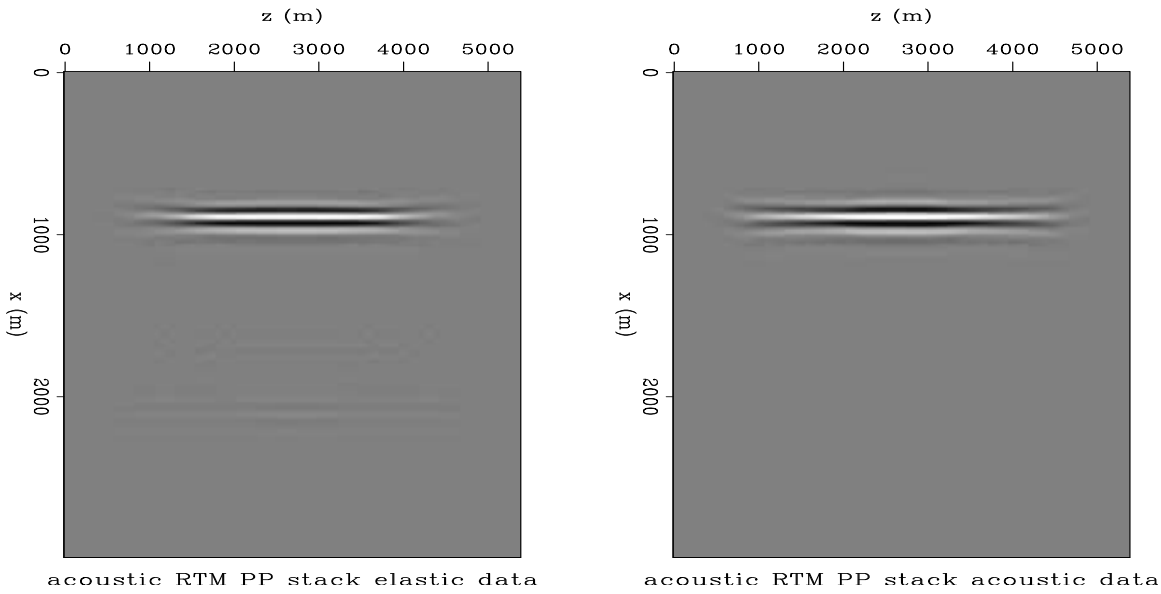

Figure 8: Comparison of the image generated by acoustic RTM of the synthetic acoustically-generated data (right) vs. acoustic RTM of the synthetic elastically-generated data (left). The images have been gained by the square of the depth and clipped at 99.7%. PZ summation is applied to the hydrophone and the vertical geophone, and the result is injected as hydrophone data only (pressure wave). Two artifacts can be seen in the migration result of the elastic data. [**ER**]

Full elastic migration results

Conceivably, since the data in Figure 5 is strictly upgoing data, and is a result of elastic Born modeling, we would expect that running elastic RTM with this data as the receiver wavefield input should produce an accurate image of the subsurface. The actual imaging results of applying the vector potential imaging condition of equation 9 to the elastic source and receiver wavefields are shown in Figure 9. Notice that each of the images has its own set of artifacts. These artifacts are the result of mode conversions occuring at the injection point of particle velocities. Whenever any particle velocity value is injected into an elastic medium, both a P and an S mode will be created, regardless of whether the recorded particle velocity was the result of a pressure or a shear wave. These modes then propagate with their respective velocities in the receiver wavefield and cross-correlate with the source wavefield at locations which are not reflector positions. They can also stack coherently over shots, as is the case here. The panels in figure 9 are not plotted at the same scale. The PS stack is an order of magnitude greater than the PP and SS stacks, and two orders of magnitude greater than the SP stack.

An interesting observation is that although each of the images in Figure 9 has different artifacts, the one thing they have in common is the true reflector position.

This feature could be used to attenuate some of the converted-mode artifacts. The one problem is that to use this criterion effectively, both the V_p and the V_s models have to be quite accurate.

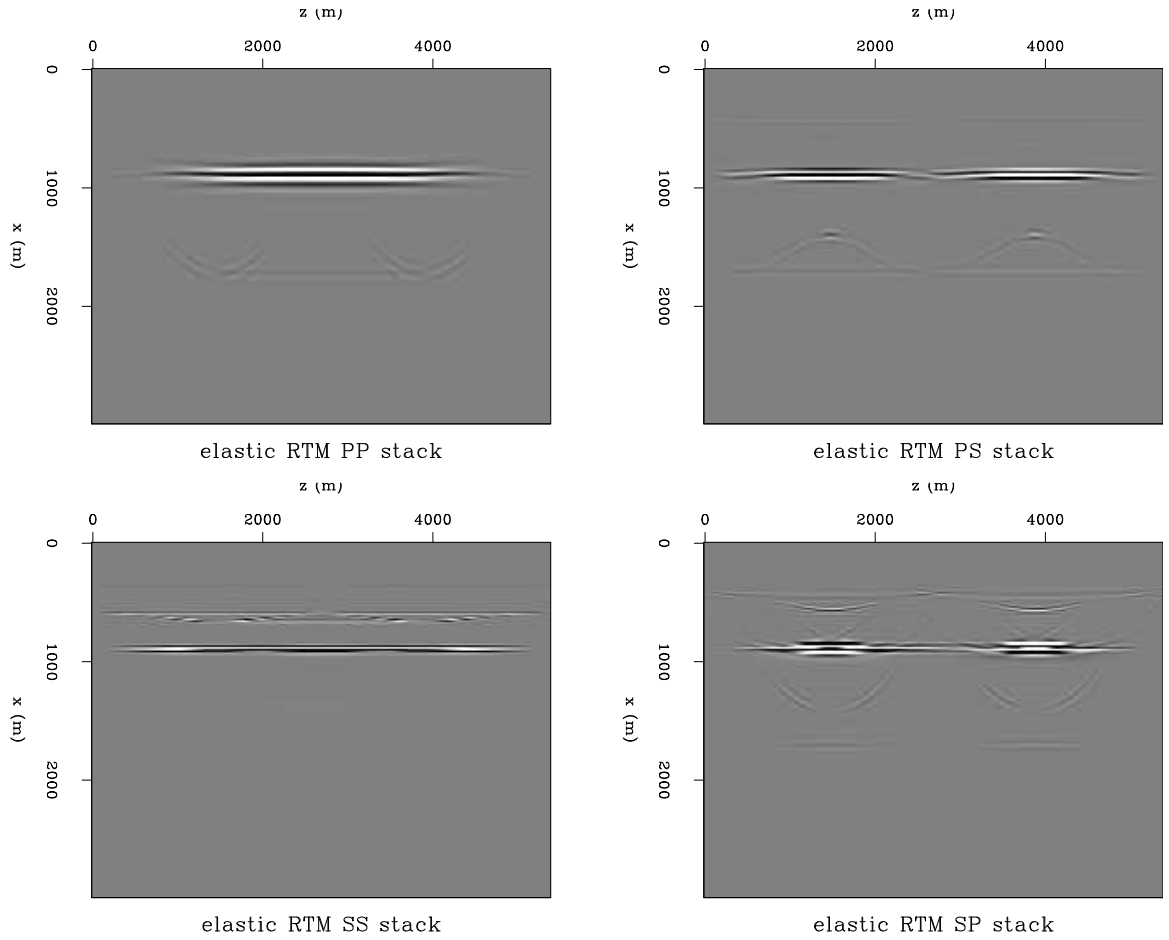

Figure 9: Images resulting from the cross-correlation of P/S source wavefield with the P/S receiver wavefield. Elastic RTM is run and the both the Born-modeled hydrophone and geophone data are injected. Top left: PP stack. Top right: PS stack. Bottom left: SS stack. Bottom right: SP stack. **NOTE** : The PS stack is an order of magnitude greater than the PP and SS stacks, and two orders of magnitude greater than the SP stack. All images have artifacts resulting from mode conversion generated at the receiver injection point. Note however that all images show the true reflector position in addition to their respective artifacts. [**ER**]

DISCUSSION AND CONCLUSIONS

The primary assumption of PZ summation for OBN data is that the vertical geophone contains only pressure wave energy. I have shown that doing a PZ summation on OBN-acquired hydrophone and vertical geophone data, where the vertical geophone component contains significant amounts of non-pressure wave data, will result

in an introduction of the non-pressure wave energy into the summation result and subsequently degrade the image. In the simple case I used, the only non-P energy was shear waves. Running acoustic RTM with shear wave data as input will invariably image the shear wave energy away from the true reflector position, since shear waves do not propagate with an acoustic velocity. However, since the shear waves have a different moveout from the pressure waves, the stacking procedure may be sufficient to remove any artifacts they may create in the image. With elastic RTM, the shear and the pressure waves may both be imaged at correct reflector positions, but additional artifacts appear as a result of mode-conversion at the data injection point.

The realism of the scenario I've modeled here can certainly be called into question. The shear velocity in the sea bottom tends to be a rather smooth gradient, which can range from a few tens of meters per second in the topmost unconsolidated sediment, to a few hundred meters per second as depth increases and the material becomes more consolidated. Therefore the very obvious P-to-S conversion in the incident wavefield (Figure 4(c)) is probably very weak. This means that the SS reflection in the Born-modeled data I've shown will be likewise very weak , and not contribute to image artifacts. The reason for choosing a minimum shear velocity of $500m/s$ was purely practical - so that the modeling grid would not have to be too fine. What could conceivably contribute to artifacts are the P-to-S conversions within the solid layers, as these are much stronger shear waves and are unaccounted for by the PZ summation's "P-only" assumption.

PZ summation is a more robust method than the methods mentioned in the introduction (Dankbaar (1985); Wapenaar et al. (1990); Amundsen (1993); Schalkwijk et al. (2003)), in that it requires less subsurface parameters to operate. It cannot however tell pressure wave energy from other energy, and assumes all data recorded on the hydrophone and vertical geophone must be P-wave energy.

I am currently working on a method which will be medium independent, and which will extract the pure pressure energy from the geophones. This hypothetical P-wave-only geophone data can be fed into the standard PZ summation in order to separate upgoing from downgoing wavefields in the data.

REFERENCES

Amundsen, L., 1993, Wavenumber-based filtering of marine point-source data: Geophysics, **58**, 1497–150.

Barr, F. J. and J. I. Sanders, 1989, Attenuation of water-column reverberations using pressure and velocity detectors in a water-bottom cable: SEG expanded abstracts, **8**, 653–656.

Beylkin, G. and R. Burridge, 1990, Linearized inverse scattering problems in acoustics and elasticity: Wave Motion, **12**, 15–52.

Dankbaar, J. W. M., 1985, Separation of p- and s-waves: Geophysical Prospecting, **33**, 970–986.

Dellinger, J. and J. Etgen, 1990, Wave-field separation in two-dimensional anisotropic media: Geophysics, **55**, 914–919.

Ronen, S., L. Comeaux, and X. Miao, 2005, Imaging downgoing waves from ocean bottom stations: SEG expanded abstracts, **24**, 963–966.

Schalkwijk, K. M., C. P. A. Wapenaar, and D. J. Verschuur, 2003, Adaptive decomposition of multicomponent ocean-bottom seismic data into downgoing and upgoing p- and s-waves: Geophysics, **68**, 1091–1102.

Virieux, J., 1986, P-sv wave propagation in heterogeneous media: Velocity-stress finite difference method: Geophysics, **51**, 889–901.

Wapenaar, C. P. A., P. Herrmann, D. J. Verschuur, and A. J. Berkhout, 1990, Decomposition of multicomponent seismic data into primary p- and s-wave responses: Geophysical Prospecting, **38**, 663–661.

Wong, M., B. L. Biondi, and S. Ronen, 2009, Inversion of up and down going signal for ocean bottom data: SEP-Report, **138**, 247–256.

Yan, J. and P. Sava, 2008, Isotropic angle-domain elastic reverse-time migration: Geophysics, **73**, S229–S239.